ELSEVIER

Physica D 80 (1995) 120–139

PHYSICA D

Transitions and kinematics of reaction–convection fronts in a cell population model

Alejandro D. Rey[a,*] Michael C. Mackey[b]

[a]*Department of Chemical Engineering, McGill University, 3455 University St., Montreal H3A 2A7, Canada*
[b]*Departments of Physiology, Physics, and Mathematics, and Centre for Nonlinear Dynamics in Physiology and Medicine, McGill University, 3655 Drummond Street, Montreal H3G 1Y6, Canada*

Received 10 May 1994; accepted 29 July 1994
Communicated by H. Flaschka

Abstract

Here we consider cell population dynamics in which there is a simultaneous proliferation and maturation. The mathematical model of this process is formulated as a nonlinear first order partial differential equation for the cell density $u(t,x)$ in which there is retardation (delay) in the temporal (t) variable. Thus we consider a transient reaction–convection equation in which the cell density is convected with maturation velocity r. For localized initial perturbations the equation has positive and negative traveling front solutions. Positive fronts correspond to the invasion of the zero amplitude solution by a finite amplitude solution, and negative fronts correspond to the reversed case. Three classes of fronts are found according to the strength of the convection velocity; (i) For strong convection ($r \gg 1$) the fronts are simple translations of the initial data, regardless of delay strength; (ii) for weak convection ($r \ll 1$) two types of fronts exist: (a) reaction–convection fronts arise if the localized initial perturbation acts at a non-zero maturation on the zero amplitude state, and (b) convection fronts arise if the localized initial perturbation acts at zero maturation on a finite amplitude state. For weak convection (cases (ii)a and (ii)b) a further classification arises according to whether the magnitude of the temporal delay is larger or smaller than a critical value τ^b. It is found that the critical delay τ^b corresponds to the Hopf bifurcation of the reaction equation that is obtained in the absence of convection ($r = 0$). For delays larger than τ^b the convective and reaction–convection fronts are oscillatory. In addition all the reaction–convection fronts reverse their direction of motion, undergo a positive to negative transition, and display non-uniform kinematics. Simulation results are validated and interpreted using solutions for the unretarded equations, and by local stability analysis.

1. Introduction

Mathematical models for a variety of biological dynamics are most appropriately framed as differential delay equations [1]. Many of these problems involve descriptions of cell replication, and in this circumstance the natural delay is the cell cycle time.

* Corresponding author.

SSDI 0167-2789(94)00174-X

In previous papers we have considered a model for cell replication in which cells are both proliferating and maturing [2–4]. The dynamics of this situation are described by the solution of a first order partial differential equation, in which there is a retardation in the time variable as well as nonlocality in the maturation variable. The computed dynamics, partially validated by local analysis, are characterized by a rich variety of spatially homogeneous and nonhomogeneous stationary modes, spatially homogeneous oscillating modes, and regular and chaotic traveling wave modes. Many of the time dependent modes were found to be directly associated with a limit cycle solution to the pure birth and death cell population balance equation [3].

In this paper we consider a simplified version of the previous model [2,3] in which the nonlocality in the maturation variable is neglected, but the dynamics are still dependent on the temporal retardation. This simplification is motivated by our desire to capture the minimal ingredients that yield the features of the more complex model. The essential ingredients of the simplified cell population model are linear convection and nonlinear reaction. The growth function in the reaction or kinetic term contains the controlling retardation or delay parameter, of essential biological relevance. As is well known, convection–reaction systems propagate fronts [5]; for convection domination the uniformly moving fronts are simple translations of the initial data, as predicted by the advection equation. Our aim here is to present a characterization of delay-induced instabilities and unsteady kinematics of propagating convection–reaction fronts, predicted by the first order delay partial differential equation. As in [2,3] it will be shown that oscillatory front propagation is associated with the presence of a limit cycle in the purely reactive equation. In Section 2, we derive the model equation, and in Section 3 we present the results of reaction–convection fronts for localized initial functions. The paper concludes with a brief discussion in Section 4.

2. Model cell population equation

A detailed description of the biological significance and mathematical derivation of a cell population model with simultaneous cell replication and maturation, and containing spatial nonlocality and temporal retardation has been given in [3,4]. The governing equations in this case are given by

$$\frac{\partial u}{\partial t} + cx\frac{\partial u}{\partial x} = D(u) + B(u_\tau)\,, \quad 0 < x \le 1\,, \quad t > 0\,, \tag{1a}$$

$$D(u) = -\delta u\,, \quad B(u_\tau) = \lambda u_\tau(1 - u_\tau)\,, \quad u_\tau = u(t - \tau, x\,\mathrm{e}^{-c\tau})\,, \tag{1b,c,d}$$

where $u(t, x)$ is the cell population with maturation x at time t, $D(u)$ is the death function, $B(u_\tau)$ is the delayed birth function, and cx is the maturation dependent convection velocity. The symbols δ and λ represent constant parameters. The nonlinear growth function contains the time delay τ and the spatial retardation $\mathrm{e}^{-c\tau}$. To complete the specification of the problem requires an initial function, taken here as

$$u(x, t) = \vartheta(x)\,, \quad (x, t) \in [0, 1] \times [-\tau, 0]\,. \tag{2}$$

In the present paper, we simplify the model by neglecting the spatial retardation in the birth function B and replace the convection velocity cx with a constant r. Without loss of generality we set $\lambda = 1$. With these modifications the equation investigated in this paper becomes

$$\frac{\partial u}{\partial t} + r\frac{\partial u}{\partial x} = -\delta u + u_\tau(1 - u_\tau)\,, \quad u_\tau = u(t - \tau, x)\,, \qquad (x, t) \in [0, 1] \times \mathbb{R}^+\,, \tag{3}$$

together with the initial function in Eq. (2). As shown in Section 2, the fixed points of the kinetics given by $D(u) + B(u_t) = 0$ are

$$u_0 = 0\,, \quad u_+ = 1 - \delta \equiv \alpha\,. \tag{4}$$

Throughout this paper u_0 represents the trivial solution and u_+ represents the spatially homogeneous steady state. Of interest here is to study the invasion of one fixed point solution by another through the propagation of a sharp front. The presence of reaction naturally leads to the invasion of the unstable fixed point u_0 by the stable fixed point u_+, here denoted by $u_+ \to u_0$. On the other hand the presence of convection leads to the invasion of stable fixed point u_+ by the unstable fixed u_0, denoted as $u_0 \to u_+$. Following [6] we denote the former as positive fronts and the later as negative fronts. In addition, for sufficiently large values of the delay parameter, it will be shown that the finite amplitude fixed point u_+ undergoes a Hopf bifurcation and becomes a limit cycle for the reaction equation ($r = 0$), and the heteroclinic trajectory then joins the zero amplitude u_0 fixed point with a limit cycle, giving rise to positive oscillatory fronts, denoted as $u(x,t) \to u_0$. The presence of convection allows for the corresponding negative case, in which the zero amplitude fixed point invades the wave solution that exists in the wake of the front, denoted as $u_0 \to u(x,t)$.

Since we wish to study front propagation, the initial functions used in this paper are time independent localized spatial perturbations of the fixed points; this class of initial functions lead to front propagation, while initial functions with small gradients usually do not lead to front propagation solutions [2,3]. The three types of initial functions $\varphi(x)$, used in this work and that lead to front propagation, are

$$\text{initial functions } (\varphi(x)): \begin{cases} \varphi_{+0}(x) = \alpha(1 - x^{1/n}) \\ \varphi_{0+}(x) = \alpha x^{1/n} \\ \varphi_{0/+}(x) = \alpha x^n \end{cases} \qquad (x,t) \in [0,1] \times [-\tau, 0],\ n \gg 1\,. \tag{5}$$

Each of the three initial functions is associated with a representative class of front propagation solutions, described below. The initial function $\varphi_{+0}(x) = \alpha(1 - x^{1/n})$, represents a perturbation on the zero amplitude solution u_0, on a narrow region in the vicinity of $x = 0$; the second initial function, $\varphi_{0+}(x) = \alpha^{1/n}$, represents a perturbation on the finite amplitude solution u_+, on a narrow region in the vicinity of $x = 0$; while the third initial function $\varphi_{0/+}(x) = \alpha x^n$, represents a perturbation on the zero amplitude solution u_0, on a narrow region in the vicinity of $x = 1$.

Since we are motivated by biological constraints, we have restricted the maturation interval $x \in [0,1]$. Therefore, in some cases, the arising front kinematics of biological interest are of transient nature. The localized nature is captured for sufficiently large values of n, here we use $5 \le n \le 10$. The boundary conditions used in this work are $u(0,t) = 0$, $t < 0$, whenever $\varphi(0) = 0$, but no conditions are enforced whenever $\varphi \neq 0$. In the numerical section of this work we use $\delta = 0.2$ and $\alpha = 1 - \delta = 0.8$ throughout. With these choices the model output, for various values of the variable parameter vector $V(r, \tau, n)$, is given by

$$u = u(x,t,V)\,, \quad (x,t,V) \in [0,1] \times \mathbb{R}^+ \times \mathbb{R}^{3+}\,. \tag{6}$$

In the remainder of this paper we study the solutions of (3) using the three initial functions (5) to obtain insight into the modes of front propagation behavior that are possible, and their dependence on the time delay τ, the convection velocity r, and the initial function $\varphi(x)$. Particular emphasis is placed on the analysis of the propagation of oscillatory fronts that arise whenever the delay strength τ exceeds a critical value τ^b. Analytical solutions for the special unretarded case ($\tau = 0$) are presented and used to identify the particular features introduced by temporal retardation. The reader is refered to [2,3] for a

detailed description of numerical methods used in this work as well as their accuracy and validation. A number of authors [7–12] have studied the global stability properties of a class of differential equations that include Eq. (3) when $\tau = 0$. These results indicate that when $\varphi(0) > 0$ the solutions of (3) (with $\tau = 0$) will be globally asymptotically stable. However when $\varphi(0) = 0$ the solutions are chaotic on a function space. The last case is of potential practical importance since chemotherapy and radiotherapy may produce states that correspond to $\varphi(0) = 0$.

2. Analytical results for the transient reaction equation ($r = 0$)

In this section we present some analytical results necessary to understand and validate the numerical solutions to Eq. (3). In the absence of convection ($r = 0$) the model equation (3) simplify to the following delay ordinary differential equation, that describes the transient kinetics:

$$\frac{du}{dt} = -\delta u + u_\tau(1 - u_\tau) . \tag{7}$$

The two fixed points of this equation are the trivial solution $u_0 = 0$ and the positive amplitude solution $u_+ = 1 - \delta = \alpha$.

2.1. Stability of the trivial solution

To examine the local stability of the trivial solution we linearize (7) about u_0 to give

$$\frac{dz}{dt} = -\delta z + z_\tau(1 - z_\tau) , \tag{8}$$

wherein $z = u - u_0$. The associated eigenvalue μ is given implicitly by

$$\mu = -\delta + e^{-\mu\tau} \tag{9}$$

and it follows that $\mu < 0$ for $\delta > 1$, $\mu = 0$ for $\delta = 1$, and $\mu > 0$ for $\delta < 1$. Thus when the zero amplitude solution u_0 is the only non-negative solution it is locally stable, and loses its stability as soon as the positive amplitude solution u_+ exists.

2.2. Stability of the positive amplitude solution

Next we examine the local stability of u_+. Again linearizing (7) about u_+ gives

$$\frac{dz}{dt} = -\delta z + (2\delta - 1)z_\tau , \tag{10}$$

where $z = u - u_+$. Assuming a time periodic solution of the form $e^{(\mu + i\omega)t}$, we obtain

$$\mu + i\omega = -\delta + (2\delta - 1)\, e^{-\mu\tau} e^{-i\omega\tau} . \tag{11}$$

Separating (11) into real and imaginary parts gives

$$\mu = -\delta + (2\delta - 1)\, e^{-\mu\tau} \cos\omega\tau , \quad \omega = (2\delta - 1)\, e^{-\mu\tau} \sin\omega\tau . \tag{12a,b}$$

For a given δ such that

$$\tau\sqrt{(2\delta - 1)^2 - \delta^2} < \cos^{-1}\left(\frac{\delta}{2\delta - 1}\right) \tag{13}$$

using the criteria of Hayes [13] it is simple to show that $\mu < 0$, and when the inequality is reversed, $\mu > 0$. Thus whenever (13) holds we know that u_+ is locally stable.

2.3. Bifurcation from u_+ to a periodic solution

It is straightforward to show that $\mu = 0$ when τ and δ satisfy

$$\tau\sqrt{(2\delta-1)^2-\delta^2} = \cos^{-1}\left(\frac{\delta}{2\delta-1}\right). \tag{14}$$

For a given δ, denote the unique solution of (14) by $\tau^b(\delta)$ This solution corresponds to a periodic solution u_p of the linear equation (10) with period

$$P = \frac{2\pi}{\omega} = \frac{2\pi\tau^b}{\sqrt{(2\delta-1)^2-\delta^2}}. \tag{15}$$

The zero in the denominator of (15) occurs at $\delta = \frac{1}{3}$. The limiting conditions of Eqs. (12) and (14) are as $\delta \to 0$, $P \to 4\tau^b = 2\pi$ and as $\delta \to \frac{1}{3}$, $P \to +\infty$ and $\tau^b \to +\infty$.

Thus when (14) is satisfied, so $\tau = \tau^b(\delta)$, there is a Hopf bifurcation from the finite amplitude solution u_+ to a periodic solution u_p of period P, given by Eq. (15). Close to the Hopf bifurcation, after initial transients die out, the periodic solutions are approximated by

$$u_p(t) \approx \alpha + \varepsilon\cos\omega t\,, \quad \varepsilon \ll 1\,. \tag{16}$$

Fig. 1 shows the bifurcation diagram in the (τ, δ) plane, obtained from (14). The full line denotes the Hopf bifurcation on which there are periodic oscillations, above which u_+ is unstable, and below which the solutions are locally stable steady states. These locally stable steady states are of two types. To the right of the $\delta = 1$ vertical line they are the trivial solutions u_0, and between the Hopf bifurcation line and $\delta = 1$ they are the positive amplitude solutions u_+. In our numerical study below we *always* use $\delta = 0.2$, which yields $\tau^b = 3.412$, $P = 11.22$.

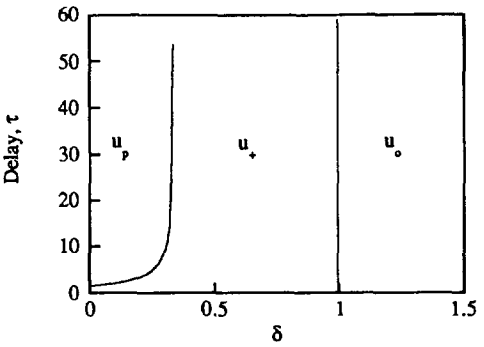

Fig. 1. Bifurcation diagram in the (τ, δ) plane, obtained from (14). The full line denotes the Hopf bifurcation on which there are periodic oscillations and above which u_+ is unstable, and below which the solutions are locally stable steady states. These steady states are of two types. To the right of the $\delta = 1$ vertical line they are the trivial solutions u_0, and to the left they are the positive amplitude solutions $u_+ = 1 - \delta = \alpha$. In the numerical solution we use $\delta = 0.1$ and $0 \le \tau \le 10$.

3. Results and discussion

The presentation of results below follows the natural classification arising from the operating time scales of the problem, given in Table 1. The multiple time scales $\{T_i\}$ operating in the partial differential equation (3), represent the elapsed time for effective change brought forth by the time delay ($T=\tau$), by convection ($T_c=1/r$), by the death rate ($T_d=1/\delta$), and by the birth rate ($T_b=1$); these last two time scales give rise to the representative time scale for net growth ($T_n=1/\alpha$). The only time scales changed in this paper are the retardation τ and the convection time scale $T_c=1/r$, with all others remaining fixed.

As is typical of multiple scale systems, we find that different characteristics regimes are obtained by changing the nature of the slowest and fastest process. When T_c is the smallest time scale, the dynamics are dominated by convection. There is no time available for significant change to occur in the restricted maturation scale ($0\le x\le 1$), and the initial data are translated without significant change. On the other hand when T_c is the slowest time scale, and the available time for significant change is therefore large, relative solution changes due to birth, death, and retardation dominate. In this case, we find that for fixed T_d and T_b ($T_b<T_d$), the distinctive temporal retardation effects on the dynamics become prominent whenever $\tau>\tau^b>T_d$, with τ^b given by (14).

Table 2 presents a summary of the different front propagation regimes, defines the nomenclature, and gives the corresponding parametric conditions in terms of the initial function ($\varphi(x)$), convection speed (r), and delay strength (τ). This classification arises naturally from the existence of the two fixed points (4), and by the presence of the multiple time scales (see Table 1). The strength of convection investigated in this paper results in two families of fronts: (a) for strong convection ($r\gg 1$) we find translating fronts (F), and (b) for weak convection ($r\ll 1$) we find (i) convection fronts (C) if the initial localized perturbation of u_+ occurs at $x=0$ and (ii) reaction–convection fronts (R) if the initial

Table 1
Time scales of the cell population model

Time scale	Delay	Convection (T_c)	Death (T_d)	Birth (T_b)	Net growth (T_n)
T	τ	$1/r$	$1/\delta$	1	$1/\alpha$

Table 2
Classification of front solutions and related parametric conditions

Exchange type (symbol)	Initial function $\varphi(x)\ 0\le x\le 1$ $-\tau\le t\le 0$	Convection speed (r)	Delay (τ)	Figure
translating fronts (F)				
$u_+\to u_0$ (F_{+0})	$\varphi_{+0}=\alpha(1-x^{1/n})$	$r\gg 1$	$\tau>0$	–
$u_0\to u_+$ (F_{0+})	$\varphi_{+0}=\alpha x^{1/n}$	$r\gg 1$	$\tau>0$	–
convection fronts (C)				
$u_0\to u_+$ (C_{0+})	$\varphi_{0+}=\alpha x^{1/n}$	$0<r\ll 1$	$0\le\tau<\tau^b$	2, 3
$u_+\to u(x,t)$ (C_{+u})	$\varphi_{0-}=\alpha x^{1/n}$	$0<r\ll 1$	$\tau>\tau^b$	3, 4
reaction–convection fronts (R)				
$t<t_0, u_+\to u_0$ $t>t_0, u_0\to u_+$ (R_{0+})	$\varphi_{0/+}=\alpha x^n$	$0<r\ll 1$	$0\le\tau<\tau^b$	5, 6, 7 8, 9, 10
$t<t_0, u(x,t)\to u_0$	$\varphi_{0/+}=\alpha x^n$	$0<r\ll 1$	$\tau^b<\tau<\tau^c$	10, 11, 12, 13

localized perturbation of u_0 occurs at $x = 1$. The table also shows that further differentiation in both convection and reaction–convection fronts occur whenever the strength of the temporal delay τ exceeds τ^b.

3.1. Translating fronts

The upper two rows of Table 2 correspond to translating fronts (F). For convection domination, the convection time scale is small ($T_c = 1/r \ll 1$) compared to the fixed reaction time scales, here given by $T_d = 1/\delta = 5$ for death, and $T_b = 1$ for birth. The two initial functions that lead to these solutions are $\varphi_{+0}(x)$ and $\varphi_{0+}(x)$, given in Eq. (5). In this case we have uniformly translating fronts that move in the $+x$ direction with constant velocity r and which, regardless of the delay τ, are accurately approximated by the solution to the linear advection equation:

$$\frac{\partial u}{\partial t} + r\frac{\partial u}{\partial t} = 0\,, \quad r \gg 1\,. \tag{17}$$

In this almost trivial case we have positive (F_{+0}) and negative (F_{0+}) fronts, given by uniform translations of the initial functions $\varphi_{+0}(x)$ and $\varphi_{0+}(x)$, respectively:

$$\textit{translating fronts}\ (r \gg 1)\begin{cases} F_{+0}\colon\ u(x,t) = \varphi_{+0}(x - rt) = \alpha(1 - (x - rt)^{1/n})\,, \\ F_{0+}\colon\ u(x,t) = \varphi_{0+}(x - rt) = \alpha(x - rt)^{1/n}\,. \end{cases} \tag{18a,b}$$

The first positive front solution represents the invasion of u_0 by u_+, while the second negative front solution represents the invasion of u_+ *by* u_0, both occurring with the constant convection speed r.

3.2. Convection fronts

The third and fourth rows in Table 2 correspond to convection fronts (C). In this case the convection velocity is small, and the reaction time constants for death ($T_d = 1/\delta$) and for birth ($T_b = 1$) are smaller than for convection ($T_c = 1/r$). For convection fronts we enforce the boundary condition $\varphi(0, t) = 0, t \in \mathbb{R}^+$. The initial function corresponding to this particular family is $\varphi_{0+}(x)$. As the name implies the fronts are driven by convection of the zero amplitude solution in the increasing maturation direction. These are then negative fronts, but a further categorization arises depending on the magnitude of the time delay. For relatively small delays such that $\tau < \tau^b$, the negative fronts (C_{0+}) correspond to the invasion of u_+ by u_0. On the other hand, for relatively strong delays with $\tau > \tau^b$, the negative fronts (C_{0u}) correspond to the invasion of a time dependent spatially non-homogeneous solution $u(x, t)$ by the zero amplitude solution u_0. Below we present numerical evidence for this behavior and provide explanations for their existence. Analytical results for the unretarded case ($\tau = 0$) provide a useful reference.

3.2.1. Analytical solutions for unretarded convection fronts ($C_{0+}, \tau = 0$)

The bifurcation diagram of Fig. 1 for the reaction equation (13) shows that for $\delta = 0.2$ and $\tau < \tau^b = 3.4$, the steady state solution u_+ is locally stable. The parametric conditions for the present regime are $r \ll 1$ and $\tau = 0 < \tau^b$. Thus we expect the translating fronts to be monotonic. In addition, for sufficiently weak delays, the solution of (3) with $\tau = 0$ provides a good asymptotic approximation to the solution for small delays ($\tau \ll 1$), and gives insight into the solution behavior for finite $\tau < \tau^b$. Using the method of characteristics we obtain, for $\tau = 0$ and $\varphi_{0+}(x)$, the following solution to Eq. (3):

$$u(x,t)=\begin{cases}\dfrac{\alpha(x-rt)^{1/n}}{e^{-\alpha t}[1-(x-rt)^{1/n}]+(x-rt)^{1/n}}; & x\geq rt\,,\\ u_0\,, & x\leq rt\,.\end{cases} \tag{19a,b}$$

The front location x^* is defined as the maturation level at which $u(x^*,t)=\alpha/2$. From (19) we find that the front position $x^*(t)$ is given by the sum of a convection and a reaction contribution:

$$x^*(t)=rt+\left(\frac{1}{1+e^{\alpha t}}\right)^n. \tag{20}$$

The first term on the right hand side of (20) is the convection contribution and the second term is the reaction contribution to the front motion. The front kinematics are defined by dx^*/dt. Eq. (20) shows that for the parameter values corresponding to this regime ($r\ll 1; n\gg 1, \alpha=o(1)$) the front velocity dx^*/dt quickly converges, in a time scale of the order $(1/\alpha)$, to the constant convection velocity r. Thus after the short lived transients die out, the front kinematics are dictated solely by the magnitude of the convection velocity r. At early times ($t\approx 1/\alpha$) the front thickness rapidly decreases and a steep shock-like front develops.

Fig. 2 shows the cell density as a function of maturation as given by Eq. (19) for $n=10$ and $r=0.01$, at three different times. The arrows indicate the direction of front motion. The fronts show a shock-like structure that is characteristic of convection-driven fronts. The shock structure arises due to the small magnitude of the convection velocity ($r\ll 1$). To maintain the front's motion, the convection term $r\,\partial u/\partial x$ must dominate over the reaction terms, and since $r\ll 1$ this leads to the shock structure ($\partial u/\partial x\gg 1$).

3.2.2. *Numerical solutions for monotonic convection fronts* (C_{0+})

The parametric conditions for this case are $r\ll 1$ and $\tau<\tau^b$. Thus we expect that the translating fronts are monotonic, and that they should be approximated by the unretarded solutions presented above when $\tau\ll 1$.

Fig. 3 shows the computed cell density $u(x,t)$ as a function of maturation x, for two different delays and several times. The arrows denote the direction of front motion. For weak delays (top) the shock solutions representing C_{0+} are completely identical to those given by Eq. (19). On the other hand, the bottom solution for $\tau=5>\tau^b$, which does not belong to this regime but is shown in this section for

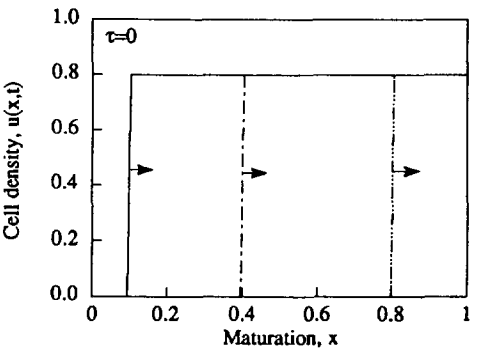

Fig. 2. Cell density $u(x,t)$ as a function of maturation x, as given by Eq. (19), for $n=10$, $\tau=0$, $r=0.01$, and corresponding to the following times t: 10 (full line), 40 (dashed-dotted line) and 80 (dashed-triple dotted line). The arrows indicate the direction of front motion. The shock-like fronts appear because convection drives the front and $\partial u/\partial x\approx o(1/r)$.

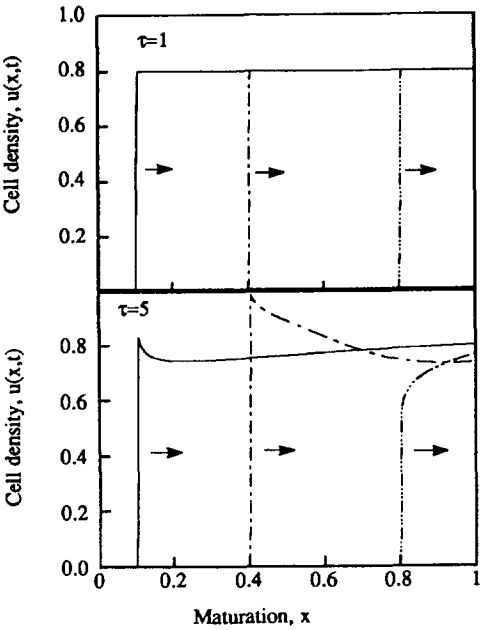

Fig. 3. Cell density $u(x, t)$ as a function of maturation x, for $r = 0.01$, $n = 10$, and $\tau = 1$ (top) and $\tau = 5$ (bottom), corresponding to the following times t: 10 (full line), 40 (dashed-dotted line), and 80 (dashed-triple dotted line). The arrows denote the direction of front motion. For small delays $\tau < \tau^b = 3.142$ the shock solutions, representative of convective fronts, are completely identical to those given by Eq. (19). On the other hand, the solution for $\tau = 5 > \tau^b = 3.412$, which is an oscillatory convective front but is shown in this section for comparative illustration, has a front velocity identical to the previous case ($\tau = 1$) but up-stream from the front it oscillates.

comparative illustration, has a front velocity identical to the previous case. However the invaded solution is now temporally oscillatory and spatially non-homogeneous. Thus we conclude that the delay strength has no effect on the solution behavior whenever $\tau < \tau^b$. Although no analytical results analogous to Eq. (20) are available for the front position for $\tau < \tau^b$, the simulations shows that the delay only modifies the reaction contribution to the front motion $x^*(t) = rt + f(t, \alpha, n, \tau)$ but again this contribution $f(t, \alpha, n, \tau)$ is negligible. The steepness of the front arises because in this regime $r \ll 1$ and for convection to drive the front, the slope must be large and of the order of $1/r \gg 1$. Hence we can conclude that for this type of front time delays do not have a significant effect on the front kinematics.

3.2.3. *Numerical solutions for oscillatory convection fronts* (C_{0u})

The parametric conditions for these negative fronts are $r \ll 1$ and $\tau > \tau^b = 3.412$. For this case the reaction equation (12) exhibits a limit cycle solution. As shown in Fig. 3b, the solutions for $\tau = 5$ describe the invasion of a time dependent spatially non-homogeneous solution $u(x, t)$ by the zero amplitude solution u_0. The front velocity is constant and equal to r. A prominent characteristic of the time dependent solution shown in Fig. 3b is the presence of two temporally oscillatory features. The temporal oscillation is reflected in: (i) the periodic changes in the slopes ahead of the shock, and (ii) in the contact point between the shock and the spatially inhomogeneous region of $u(x, t)$. For the selected times the figure shows that this point oscillates between $u = 0.6$ and $u = 1$. Since $r \ll 1$, we expect that whenever $u_p(t)$ exists it will be weakly perturbed by the small convection effect.

To understand the nature and origin of this unusual front solution, characterized by a shock structure

connecting an oscillatory and spatially non-homogeneous solution with the trivial u_0 amplitude solution, we integrated the reaction equation (7) using the initial conditions $\varphi_{0+} = \alpha\zeta^{1/n}$, $0 \le \zeta \le 1$ and compared the results with the solution to the full convection–reaction equation (3), for a wide range of $V = (r, \tau, n)$ values. This integration is identical to integrating (3) along its characteristics, $x = \zeta + rt$, for the trivial case $r = 0$. By momentarily focusing on the dynamics generated by the reaction terms, we find the source of the complexity shown in Fig. 3b.

Fig. 4 shows the cell density $u(x, t)$ as a function of maturation x (full line) on the right scale, and the retarded $u_\tau(1 - u_\tau)$ (dashed-triple dotted line) and unretarded $u(1 - u)$ (dashed-dotted line) birth functions as a function of maturation on the left scale, for $r = 0.001$, $\tau = 3.6$, and $n = 10$. The open arrows indicate the corresponding axes for each curve. The selected early times are indicated in each plot and the delay is now slightly large than $\tau^b = 3.4$. The dashed line represents the solution to the reaction equation (7). At this early times the shock forms close to $x = 0$ and, driven by convection, starts moving in the $+x$ direction. The figures show that up-stream from the front the solutions are spatially monotonic since the driving force $u_\tau(1 - u_\tau)$ is monotonic. The fact that up-stream from the

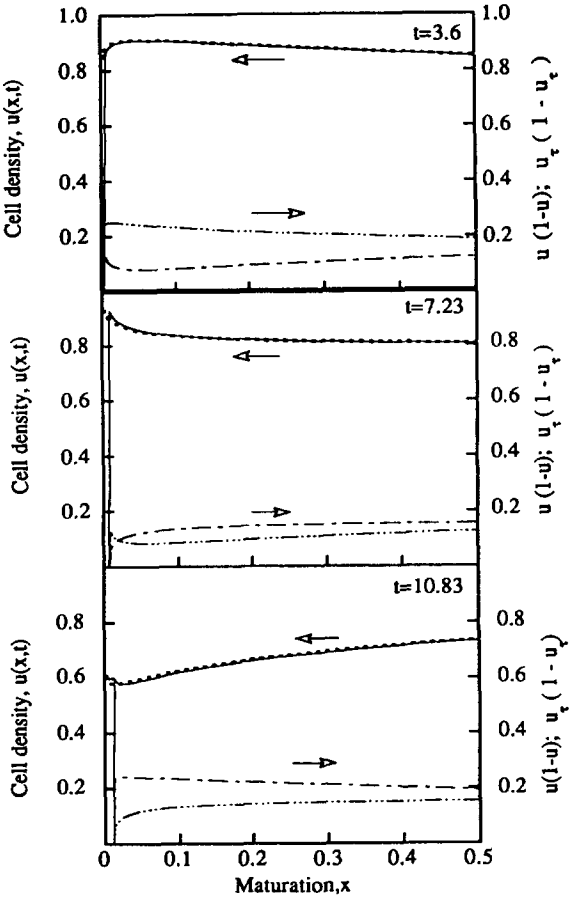

Fig. 4. Cell density $u(x, t)$ as a function of maturation x (full line) on the left scale, and the retarded $u_\tau(1 - u_\tau)$ (dashed-triple dotted line) and unretarded $u(1 - u)$ (dashed-dotted line) birth functions as a function of maturation on the right scale, for $r = 0.001$, $\tau = 3.6 > \tau^b = 3.412$, and $n = 10$. The open arrows indicate the corresponding axes for each curve. The times are indicated in each plot. The dashed line represents the solution to the reaction equation (7).

front the slopes oscillate is explained by focusing on the effect of the existing retarded birth $u_\tau(1-u_\tau)$ compared with the unretarded birth $u(1-u)$. Due to the delay, the up-stream solution is above (below) u_+ whenever the retarded birth is larger (smaller) than the unretarded birth. The figure also shows that the solutions to Eqs. (3) and (7) are only spatially shifted but otherwise identical. The solution to the reaction–convection equation is shifted to the right by the maturation distance $x = rt$ due to the convection effect, exactly as predicted by the method of characteristics [5] applied to our first order hyperbolic partial differential equation (3).

In partial summary, we have shown that if the convection is weak ($r \ll 1$) and the temporal retardation large ($\tau > \tau^b$) the solutions to (3) are slow propagating shocks in which the zero amplitude solution invades a strongly temporally oscillating and spatially nonhomogeneous solution. The origin of the oscillations has been identified and lies entirely in the reaction terms of (3).

3.3. Reaction–convection fronts

The last two rows in Table 2 correspond to reaction–convection fronts (R). In this case the convection velocity is again small, and the reaction time constant for death ($T_d = 1/\delta$) and birth ($T_b = 1$) are smaller than for convection ($T_c = 1/r$). For reaction–convection fronts we use the boundary condition $\varphi(0, t) = 0$, $t \in \mathbb{R}^+$ to capture the competition between the right traveling convection of u_0 with the left traveling reaction front. As the name implies the fronts are driven by both reaction and convection, and are obtained when using the initial function $\varphi_{0/+}(x) = \alpha x^n$. Since u_0 is unstable, it will be invaded by a finite amplitude solution and the resulting positive front will move in the $-x$ direction. On the other hand the u_0 solution is convected in the $+x$ direction with a speed r and the resulting interaction of the positive front and the convective motion gives rise to a reversal in the front's direction motion. The collision between the convection driven u_0 steady state and the reaction driven front results in an unusual front transition, at which positive fronts become negative fronts. The time (t_0) and location ($x^*(t_0)$) for the front transition depend strongly on the magnitude of r. The kinematics are now of accelerating and decelerating type. For relatively weak delays, $\tau < \tau^b$, the positive and negative fronts (R_{+0}) correspond to the invasion of u_0 by u_+ followed by the reverse invasion. On the other hand, for strong delays such that $r > \tau^b$, the negative fronts (R_{0u}) correspond to the invasion of the zero amplitude solution u_0 by a time dependent spatially non-homogeneous solution $u(x, t)$ if $t < t_0$, followed by a withdrawal when $t > t_0$. Below we present numerical evidence and further explanations for these phenomena.

3.3.1 Analytical solutions for unretarded reaction-convection fronts ($R_{0+}, \tau = 0$)

The bifurcation diagram of Fig. 1 for the reaction equation (13) shows that when $\delta = 0.2$ and $\tau < \tau^b = 3.412$, the u_+ solution is stable. The parametric conditions for the present regime are $r \ll 1$ and $\tau = 0 < \tau^b$. Thus we expect monotonic translating fronts. For sufficiently small delays, the solution of (3) with $\tau = 0$ provides a good asymptotic approximation. Using the method of characteristics we obtain, for $\tau = 0$ and $\varphi_{0/+}(x)$, the following solution to Eq. (3):

$$u(x,t) = \begin{cases} \dfrac{\alpha(x-rt)^n}{e^{-\alpha t}[1-(x-rt)^n] + (x-rt)^n}\,; & x \geq rt\,, \\ u_0\,, & x \leq rt\,. \end{cases} \tag{21a,b}$$

To find the driving forces governing the front kinematics we again define the front location x^* as the

maturation location at which $u(x^*, t) = \alpha/2$. With this definition, Eq. (21) predicts that the front position x^* is given by the sum of a convection contribution and a reaction contribution:

$$x^*(t) = rt + \left(\frac{1}{1+e^{\alpha t}}\right)^{1/n}. \tag{22}$$

For the parameters of this regime ($r \ll 1$, $n \gg 1$, $\alpha = o(1)$) it is seen that at early times reaction controls the positive front motion, but at intermediate times the increasing convection matches the decreasing reaction effect, resulting in a direction reversal of the front's motion at time $t = t_0$ when $dx^*/dt = 0$. An explicit approximation for t_0, whenever $t_0 > \alpha$ is

$$t_0 = \frac{n}{r}\ln\left(\frac{\alpha}{nr}\right). \tag{23}$$

As $r \to 0$ the limits of (22) and (23) are, $t_0 \to +\infty$ and $x^*(t_0) \to 0$. Eq. (22) shows for $t > t_0$, the front kinematics are governed by convection and the front velocity converges to the convection speed. Fig. 5 shows the front position x^* as a function of time (full line) and the front velocity as a function of time (dashed line), for $r = 0.01$, $n = 10$, and $\tau = 0$. The arrows indicate the corresponding axes. For this values $t_0 = 26.03$ and $x^*(t = t_0) = 0.385$. The figure shows that when $t > t_0$ the front velocity asymptotes to the convection speed $r = 0.01$. Fig. 6 shows the corresponding cell density $u(x, t)$ as a function of maturation for three different times. The arrows now indicate the direction of front motion. At early times ($t < t_0 = 4.01$) the positive front decelerates, at $t = 28.04 \approx t_0$ the front has just reversed it's direction of motion, and for $t > t_0$ the negative front accelerates up to the convection speed. The front exits at time $t_e = 1/r = 100$. The figure shows that the positive fronts are spread out due to the dominance of reaction, but the negative fronts driven by convection have the same shock structure as the convection fronts. Thus for $t > t_0$ and $\tau = 0$ the reaction–convection fronts become identical to the convection fronts.

3.3.2. *Numerical solutions for monotonic reaction–convection fronts* (R_{0+})

In this regime since $\tau < \tau^b$, we expect monotonic fronts, and if τ is sufficiently small we expect that Eq. (21) will provide a good approximation. Fig. 7 shows the computed cell density $u(x, t)$ as a function of maturation x for three different times. The arrows denote the direction of front motion. The front

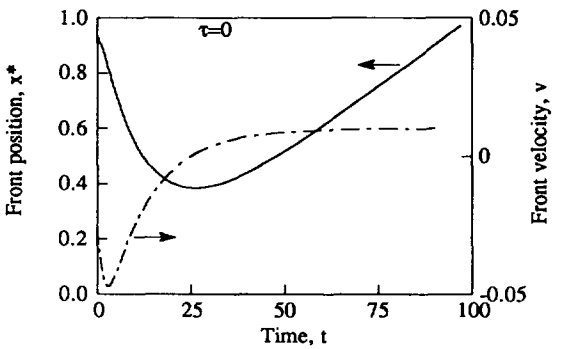

Fig. 5. Front position x^* (full line) and front velocity (dashed line) as a function of time, for $r = 0.01$, $n = 10$, and $\tau = 0$. The arrows indicate the corresponding axes. For these values front reversal occurs at $t_0 = 26.03$ and $x^*(t = t_0) = 0.385$. The figure shows that when $t > t_0$ the front velocity is asymptotic to the convection speed $r = 0.01$.

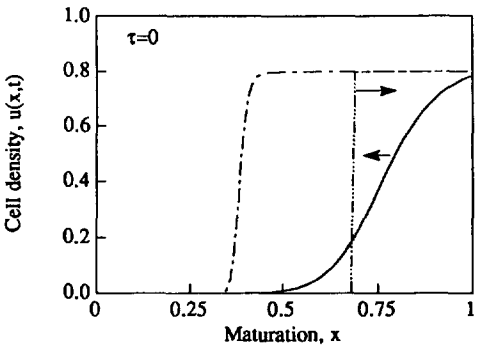

Fig. 6. Cell density $u(x,t)$ as a function of maturation for times t: 4.01 (full line), 28.04 (dashed-dotted line), and 68.01 (dashed-triple dotted line) with the parameters as in Fig. 5. The arrows now indicate the direction of front motion. At early times ($t < 4.01$) the positive front decelerates, at $t = 28.04 \approx t_0$ the front has just reversed the direction of motion, and for $t > t_0$ the negative front accelerates up to the convection speed. The front exits by crossing $x = 1$ at time $t_e = 1/r = 100$.

with no arrow corresponds to a time $t = 28.82 \approx t_0$. For weak delays, the fronts remain heteroclinic trajectories between u_0 and u_+. Although no analytical results, as in Eq. (20), were obtained for the front kinematics for $\tau \neq 0$, the simulations show that the delay only modifies the reaction contribution to the front motion as in Eq. (23), but in contrast to the convection front regime this contribution controls the front motion as τ increases. The delay effect ($\tau > \tau^b$) on kinematics will be discussed further in the next section, where stronger delay regimes are discussed. The steepness of the front that develops for $t > t_0$ arises because in this regime $r \ll 1$, and for convection to drive the front, the slope must be large and of the order of $1/r \gg 1$.

Fig. 8 shows the front position x^* as a function of time for three different convection velocities. The figure shows the trends captured by Eqs. (22), (23). As r decreases the fronts penetrate further into the small maturation region, but the retraction from this region is slower. Fig. 9 shows the corresponding cell density $u(x,t)$ as a function of maturation at front reversal. Note that the front steepness increases for decreasing r.

For this regime, we also found that when $\tau < \tau^b$, the fronts are monotonic. The main effect of the delay is to gradually slow the kinematics, and reduce the penetration distance $d = 1 - x^*(t_0)$ (see Fig. 8

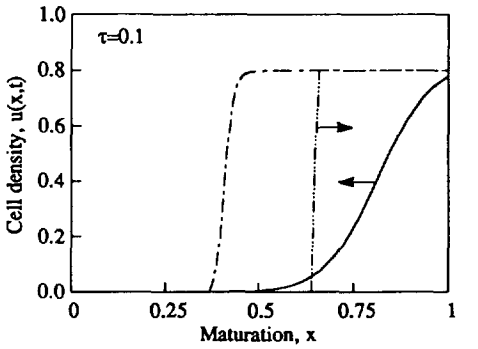

Fig. 7. Cell density $u(x,t)$ as a function of maturation x, for $r = 0.01$, $n = 10$, and $\tau = 0.1$ at the times t: 3.2 (full line), 28.82 (dashed-dotted line), and 64 (dashed-triple dotted line). The arrows denote the direction of front motion. The front with no arrow corresponds to a time $t = 28.82 \approx t_0$. For delays $\tau < \tau^b = 3.412$, the fronts are monotonic.

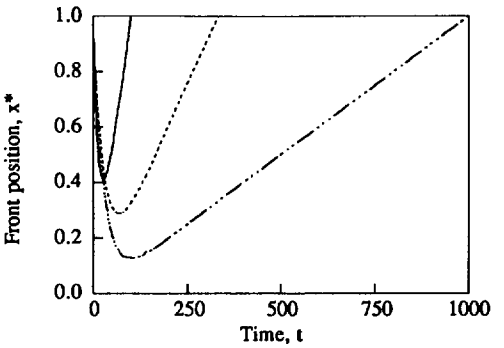

Fig. 8. Front position x^* as a function of time for $\tau = 0.1$, $n = 10$, corresponding to the following convection velocities r: 0.01 (full line), 0.003 (dashed line), and 0.001 (dashed-triple dotted line). The figure shows the trends captured by Eqs. (24), (25). Namely, as r decreases the fronts penetrate closer to $x = 0$, and their retraction is slower.

below). When τ is sufficiently close to τ^b, pretransitional decaying oscillations are observed, since the nature of u_+ is that of an attracting spiral fixed point.

3.3.4. Numerical solutions for oscillatory reaction–convection fronts (R_{0u})

The parametric conditions for these fronts are $r \ll 1$ and $\tau > \tau^b = 3.4$. For this case the reaction equation (7) exhibits a limit cycle solution. As mentioned above, increasing τ slows the positive front kinematics and reduces the distance at which there is motion reversal. Fig. 10 shows the computed front position x^* as a function of time and the corresponding front velocity, for $r = 0.01$, $n = 10$, and for three different delays. The figures clearly show the trends for increasing delay magnitudes. At sufficiently low τ, the fronts penetrate further and the kinematics follow that of the unretarded case (Eqs. (22), (23)). For larger τ the penetration toward $x = 0$ is greatly reduced, and the kinematics are slower. For sufficiently large delays $\tau > \tau^c$, the fronts do not penetrate and the solution evolves to u_0.

Fig. 11 shows the cell density $u(x, t)$ as a function of maturation x, for $r = 0.001$, $\tau = 3.6 > \tau^b$, and $n = 10$, and for three different times. For $\tau > \tau^b$ the kinetics has a limit cycle and the observed oscillations clearly reflect this fact. The fronts are now heteroclinic loops joining u_0 and u_p. The arrows in the figures denote the direction of front motion; for $t < t_0 = 72$ the positive fronts have an oscillatory wake with a wave length that increases for increasing distances from the front. At $t = t_0$ the front comes

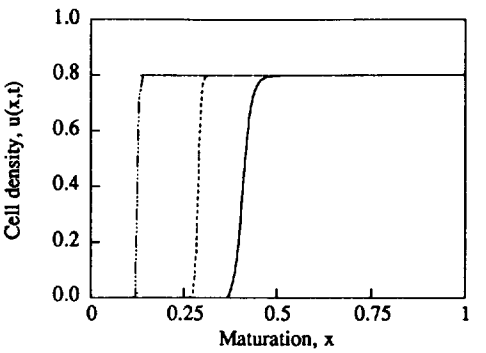

Fig. 9. Cell density $u(x, t)$ as a function of maturation at front reversal ($t = t_0$). The parameters are as in Fig. 8. The corresponding location and times are (x^*, t_0): (0.41, 28.82); (0.288, 70), and (0.128, 110). Note that the front steepness increases for decreasing r.

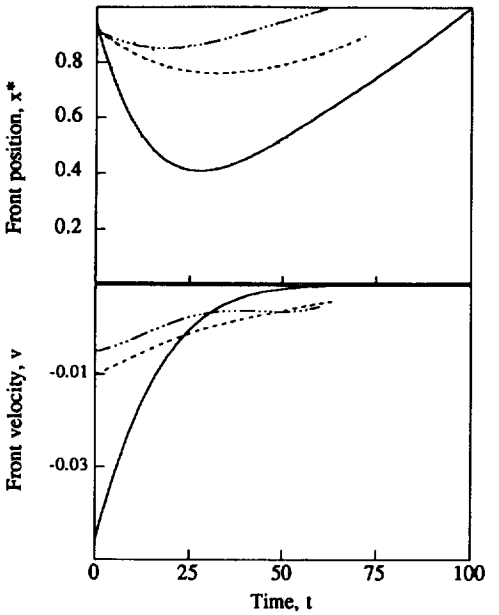

Fig. 10. Front position x^* as a function of time and corresponding front velocity dx^*/dt, for $r = 0.01$, $n = 10$, and for the following delays τ: 0.1 (full line), 3.6 (dashed line), and 10 (dashed-triple dotted line). At low τ, the fronts penetrate further and the kinematics follow that of the unretarded case (Eqs. (24), (25)). For larger τ the penetration is greatly reduced, and the kinematics are slower. For sufficiently large delays, $\tau > \tau^c \approx 11$ the fronts do not penetrate and the solution evolves to u_0 (see Fig. 14).

to a halt and with a more refined spatial structure in the wake. Finally for $t > t_0$ the gradual refinement of the spatial structure continues as the front moves, driven by convection, to exit at $x = 1$. We have performed extensive computations for this regime and Fig. 11 is representative for this regime. Similar types of oscillatory fronts can be found in other reaction–diffusion models [14], and in the KdV equation [15]. We have found that as $r \to 0$, i.e. as the perturbation of the reaction equation weakens, the penetration distance increases and the wave length of the oscillation tends to zero. We note that the negative fronts have the typical shock-like structure of convection driven fronts whenever $r \ll 1$.

To understand the nature and origin of these front solutions we integrated the reaction equation (7) using the initial conditions $\varphi(\zeta) = \alpha\zeta^n$, $0 \le \zeta \le 1$, and compared the results with the solution to the full convection–reaction equation (3) for $\varphi_{0/+}(x) = \alpha x^n$ and a wide range of $V = (r, \tau, n)$ values. Fig. 12 shows the cell density $u(x, t)$ as a function of maturation x (full line) on the right scale, and the retarded $u_\tau(1 - u_\tau)$ (dashed-triple dotted line) and unretarded $u(1 - u)$ (dashed-dotted line) birth functions as a function of maturation on the left scale. The open arrows indicate the corresponding axes for each curve. The dotted line corresponds to the numerical integration of Eq. (7) for the same parameters. The time intervals are chosen to be 5τ. The selected times are indicated in each plot and the delay is now slightly larger than $\tau^b = 3.412$. At early times the front forms close to $x = 1$ and start moving, driven by reaction, in the $-x$ direction. The figures show that at $t = 18$ and up-stream from the front, the solution is u_0 since the driving force $u_\tau(1 - u_\tau)$ is zero. The fact that the wake of the front oscillates is explained by focusing on the effect of the existing retarded birth $u_\tau(1 - u_\tau)$ as compared to the unretarded birth $u(1 - u)$. Due to the delay, the solution in the wake is above (below) u_+ whenever the retarded birth is larger (smaller) than the unretarded birth. In contrast to the oscillating convection

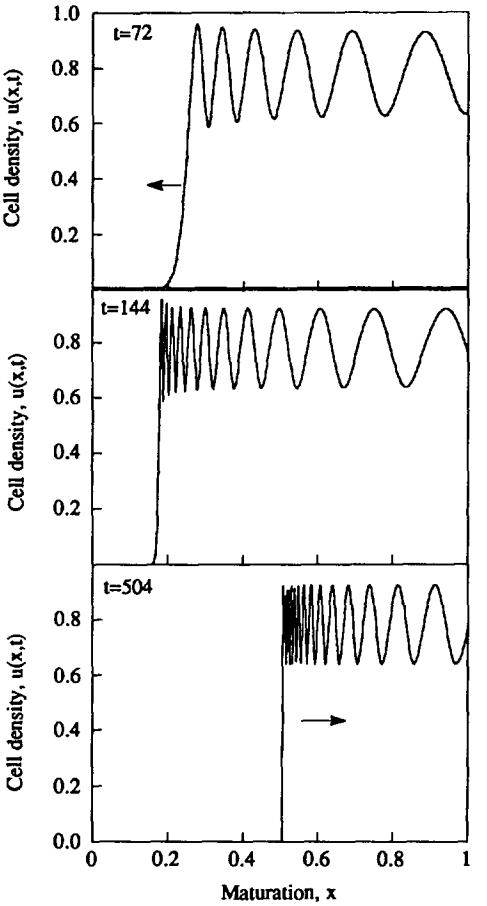

Fig. 11. Cell density $u(x, t)$ as a function of maturation x for $r = 0.001$, $\tau = 3.6 > \tau^b$, and $n = 10$, and for three times t: 72 (top), 144 (middle), and 504 (bottom). For $\tau > \tau^b$ the kinetics show limit cycle behavior and the observed oscillations clearly reflect this fact. The arrows in the figures denote the direction of front motion. For $t = 72 < t_0 = 144$ the positive fronts have an oscillatory wake with a wave length that increases for increasing distances from the front. At $t = t_0 = 144$ the front comes to a halt and has a more refined spatial structure in the wake. Finally at $t > t_0$ the gradual refinement of the spatial structure continues as the front moves in the $+x$ direction, driven by convection, to exit at $x = 1$.

fronts (C_{0u}), the function $u_\tau(1 - u_\tau)$ is oscillatory instead of monotonic (on $0 \leq x \leq 1$) and always lags the unretarded function $u(1 - u)$. The dotted line representing the solution in the absence of convection exhibits the same oscillations, and again the only effect of the weak convection is a simple spatial shift, as in the case of oscillating convection fronts. For example, at $t = 36$, if we translate the front predicted in the absence of convection to the right by $rt = 0.36$ we recover the wake predicted in the presence of weak convection. Note that as time increases the wave length of the peaks next to the front decrease. The bottom figure clearly shows the origin of structure refinement for $r > 0$. Since $t = 36 > t_0$ the front has already reversed its motion and now moves to the left, but the second peak in the front's wake is still moving to the right, as seen by comparing its position at $t = 54$ with that at $t = 36$. The net effect is then that the front reverses its motion but the wave in the wake of the front still travels to left, resulting in a wave length decrease. This wave length decrease is a function of the distance from the front since

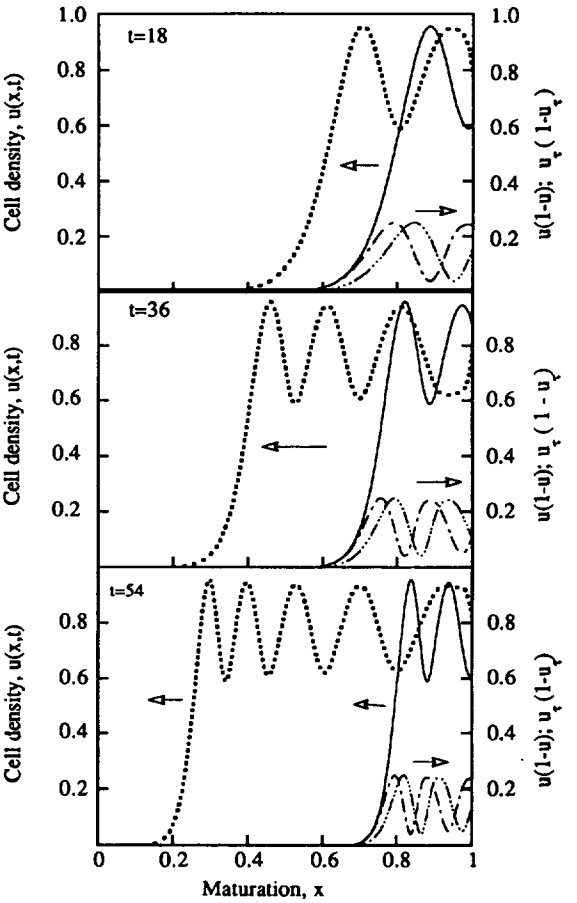

Fig. 12. Cell density $u(x,t)$ as a function of maturation x (full line) on the left scale, and the retarded $u_\tau(1-u_\tau)$ (dashed-triple dotted line) and unretarded $u(1-u)$ (dashed-dotted line) birth functions as function of maturation on the right scale, for $r=0.01$, $\tau=3.6>\tau^b=3.412$, and $n=10$. The open arrows indicate the corresponding axes for each curve. The dotted line corresponds to the numerical integration of Eq. (7) for the same parameters. The chosen time intervals are equal to 5τ.

before the motion reversal the waves were shorter closer to the front. All these observations also hold for Fig. 11.

Fig. 13 shows the cell density $u(x,t)$ as a function of maturation x for $n=10$ (top) and $n=5$ (bottom). The figure shows that increasing n, thus decreasing the length scale of the local perturbation, affects the transient kinematics of the reaction–convection fronts. For larger n the penetration distance is smaller as predicted by Eq. (22). On the other hand the figure also shows that, after the initial transient dies out, the oscillations are shifted but of similar wave length.

3.3.5. Perturbation dissipation and strong delays

As shown in Fig. 10, if τ is too large, fronts do not propagate, the initial perturbation is dissipated, and the solutions evolve towards u_0. Fig. 14 shows the cell density $u(x,t)$ as a function of maturation x (full line) on the left scale, and the retarded (dashed-triple dotted line) and unretarded (dashed-dotted line) birth functions as a function of maturation on the right scale, for $r=0.01$, $\tau=10>\tau^c$, and $n=10$.

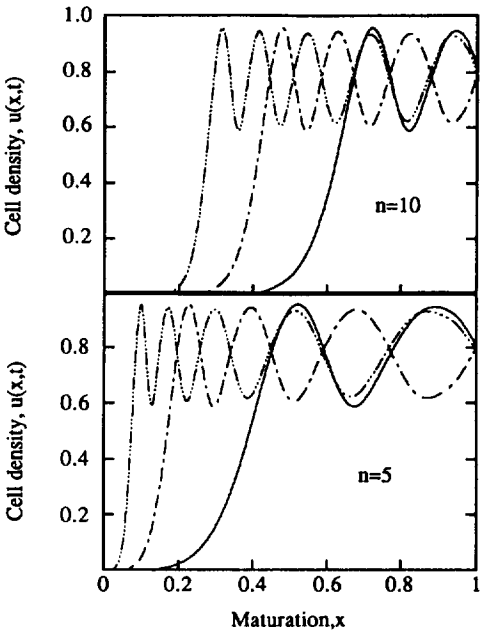

Fig. 13. Cell density $u(x,t)$ as a function of maturation x, for $r = 0.01$, $t = 3.6$, $n = 10$ (top) and $n = 5$ (bottom). The corresponding times are t: 18 (full line), 36 (dashed-dotted line), and 54 (dashed-triple dotted line). The figure shows that increasing n, and thus decreasing the length scale of the local perturbation, affects the transient kinematics of the reaction–convection fronts. For larger n the penetration toward $x = 0$ is smaller, in agreement with Eq. (24). After the initial transient dies out, the oscillations are shifted but of similar wave length.

The arrows indicate the corresponding axes for each curve. The figure shows that large delays produce a birth rate that cannot sustain growth, as seen by a direct comparison of the retarded birth function $u_\tau(1-u_\tau)$ with the unretarded birth function $u(1-u)$. Thus although an increase in the strength of the delay refines the structure of the front solution, there is a threshold above which insufficient growth occurs. A rough estimate of τ^c is obtained by requiring the death rate to be equal to the initial retarded birth:

$$\delta u = \varphi(x - r\tau) \times (1 - \varphi(x - r\tau)) . \tag{24}$$

Using the representative value $u = \alpha/2$ and the appropriate initial condition, we find for $n = 10$ and $\delta = 0.2$ that the predicted $\tau^c = 11$, in sufficiently good agreement with the simulation results.

4. Conclusions

Cell population models consisting of first order partial differential equations with temporal and spatial retardations were previously shown to predict a rich variety of phenomena. In this paper we have shown that a simplification of the more complex model, containing only temporal retardations, displays an interesting family of front propagation solutions depending on the magnitude of convection and the temporal delay. In the strong convection limit, the model reduces to the advection equation, which just translates initial data. On the other hand, for weak convection and relatively simple

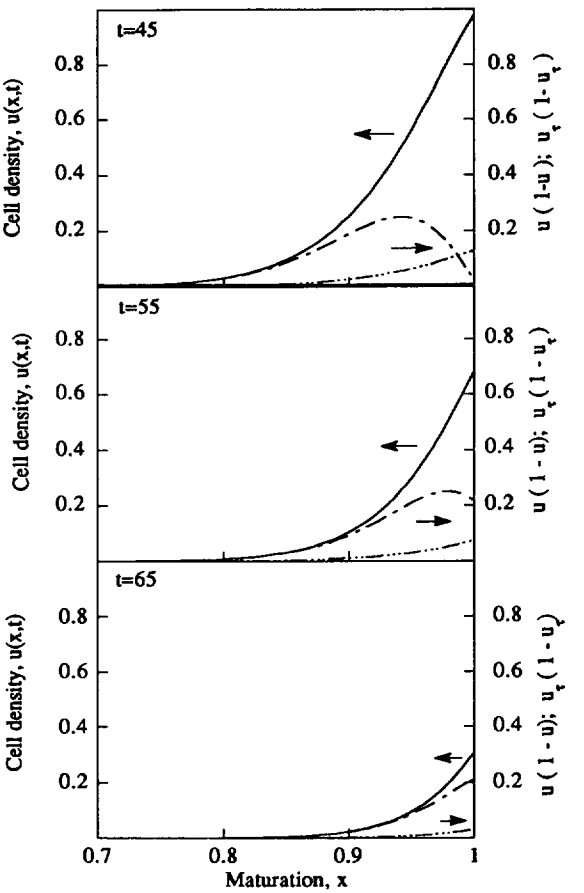

Fig. 14. Cell density $u(x, t)$ as a function of maturation x (full line) on the left scale, and the retarded (dashed-triple dotted line) and unretarded (dashed-dotted line) birth functions as a function of maturation on the right scale, for $r = 0.01$, $\tau = 10 > \tau^b = 3.412$, and $n = 10$. The arrows indicate the corresponding axes for each curve. The figure shows that large delays produce a birth rate that cannot sustain growth, as seen by a direct comparison of the retarded birth function $u_\tau(1 - u_\tau)$ with the unretarded birth function $u(1 - u)$.

nonlinear reaction kinetics, front propagation may be driven by convection or it may be driven by a changing competition between convection and reaction. The change in competition results in the reversal of front motion. Both types of convection and reaction–convection fronts exhibit temporal and spatial oscillatory behavior whenever the delay exceeds a critical value. This critical value corresponds to a Hopf bifurcation of the reaction equation. The structure of the oscillatory reaction-convection fronts is finer when convection is weaker.

Recently it has become possible to modify various parameters related to the cell maturation/proliferation process using techniques from molecular biology. Extensions of the results of this work provide theoretical predictions that are, for the first time, potentially testable. In the process we stand to greatly expand our knowledge on the dynamics of the cell replication process. This will be the subject of a later paper.

Acknowledgments

We thank the McGill University Computing Center for a grant to defray the computational costs of this research and the Natural Sciences and Engineering Research Council (Canada) for Operating Grant support to both ADR and MCM. MCM also thanks NATO, the Royal Society of London, and the Alexander von Humboldt Stiftung for support.

References

[1] M.C. Mackey and J.G. Milton, Comments Theor. Biol. 1 (1990) 299.
[2] A.D. Rey and M.C. Mackey, Chaos 2 (1992) 231.
[3] A.D. Rey and M.C. Mackey, Can. Appl. Math. Quart. 1 (1993) 61.
[4] M.C. Mackey and R. Rudnicki, J. Math. Biol., in press.
[5] B. Finlayson, Numerical Methods for Problems with Moving Fronts (Ravena Park Publishing, Washington, 1992).
[6] M.C. Cross and P.C. Hohenberg, Rev. Mod. Phys. 65 (1993) 851.
[7] A. Lasota, Nonlin. Anal. 5 (1981) 1181.
[8] P. Brunovsky, Nonlin. Anal. 7 (1983) 167.
[9] P. Brunovsky and J. Komornik, J. Math. Anal. Appl. 104 (1984) 235.
[10] R. Rudnicki, Ergod. Theor. Dynam. Syst. 5 (1985) 437.
[11] R. Rudnicki, Bull. Pol. Acad. Sci. Math. 35 (1987) 289.
[12] K. Loskot, J. Diff. Eqns. 58 (1985) 1.
[13] N.D. Hayes, J. London Math. Soc. 25 (1950) 226.
[14] J.A. Sherratt, Physica D 70 (1994) 370.
[15] V.I. Karpman, Non-linear Waves in Dispersive Media (Pergamon, Oxford, 1975).